Supplementary Information for

Cycling and persistence of iron-bound organic carbon in subseafloor sediments

Yunru Chen[1,2], Liang Dong[3], Weikang Sui[3], Mingyang Niu[1], Xingqian Cui[3], Kai-Uwe Hinrichs[2,4], Fengping Wang[1,3,5*]

1. State Key Laboratory of Microbial Metabolism, School of Life Sciences and Biotechnology, Shanghai Jiao Tong University, Shanghai 200240, China

2. MARUM-Center for Marine Environmental Sciences, University of Bremen, D-28359 Bremen, Germany

3. Key Laboratory of Polar Ecosystem and Climate Change, Ministry of Education, and School of Oceanography, Shanghai Jiao Tong University, Shanghai 200240, China

4. Faculty of Geosciences, University of Bremen, D-28359 Bremen, Germany

5. Southern Marine Science and Engineering Guangdong Laboratory (Zhuhai), Zhuhai 519000, China

*Correspondence: fengpingw@sjtu.edu.cn

This file includes:

Supplementary Discussion

Variations of TOC and Fe_R-OC records over glacial-interglacial cycles

Because of relatively weak microbial activities and well-established age model, core QDN-G1, representing typical continental slope sediments, was used to constrain the influence of TOC and Fe_R-OC depositional history over glacial-interglacial cycles on their sedimentary records.

In global marine sediments, except polar regions, the burial of OC has natural variations over glacial-interglacial cycles, with much higher accumulation rate in glacials than during interglacials for higher marine primary productivity and more efficient preservation[1]. If the environmental factors being the main controlling factor of OC content, higher content should be expected in glacials. However, in core QDN-G1, we found consistently low TOC and Fe_R-OC content across MIS 5 (interglacial) and MIS 4 (glacial) (Supplementary Fig. 6b).

The variations in the carbon isotope ratio of OC in marine sediments are generally ascribed to three reasons: variable contribution of terrestrial- and marine-sourced OC (sediment provenance), variable isotope composition of marine-sourced OC and selective microbial degradation after deposition[2]. If the carbon isotope ratio reflects the relative contribution of terrestrial and marine OC, it should be in lower in MIS 2 and MIS 4, when the sea-level stand was at least 40 meters lower than that in MIS 5 (Supplementary Fig. 6e) and terrestrial supply was higher for the closer river mouth to

the study sites[3]. However, the carbon isotope ratio of TOC and Fe_R-OC were consistently depleted during MIS 5 to MIS 4 and became more enriched during MIS 3 to 1 (Supplementary Fig. 6c). Therefore, the variations can be hardly explained by the changes in sediment provenance. If it reflects variation in the isotope composition of marine OC, we should also expect lower values in interglacials (MIS 1 and MIS 5) and lower values in glacial (MIS 2 to MIS 4)[4]. Similarly, this possibility is also ruled out.

Collectively, the distinctive low content and depleted carbon isotope ratio of TOC and Fe_R-OC can be hardly explained by the depositional history on glacial-interglacial timescale.

Supplementary Table 1. AMS ^{14}C age control points used to reconstruct the age model of core QDN-G1

Depth (cmbsf)	AMS ^{14}C age (BP)	Error (BP)	Calendar Age (cal BP)	Dating foraminifera species
0	2030	±30	1603	*G. ruber*
80	8090	±30	8538	*G. ruber*
120	10500	±30	11657	*G. ruber*
200	14050	±40	16457	*G. ruber*
280	21070	±70	24878	*G. ruber*
360	27450	±120	31069	*G. ruber*
400	30810	±170	34387	*G. ruber*

Supplementary Table 2. The input parameters for geochemical modelling of net sulfate reaction rate after the MATLAB script of Wang et al. 2008[5].

Parameters	Value for core QDN-G1	Value for core QDN-14B	Unit
Porosity	0.7	0.7	\
Formation factor	2.2	2.2	\
Sedimentary rate near the seafloor	0.000115	0.000115	m yr^{-1}
Diffusivity	0.0175	0.0175	m^2 yr^{-1}
External flow advection velocity	0.00001	0.00001	m yr^{-1}
Significance level (two-sided F-test)	0.05	0.05	\
Minimum number of measured data within each reaction zone	3	3	\
Relative precision of concentration measurements	0.01	0.01	\
Number of random concentration profiles to estimate the uncertainty of reaction rates	50	50	\
Temperature	4	4	℃
Pressure	147.8	137.0	bar
Salinity	35	35	\
Water depth	1478	1370	m
Dry bulk density	0.9	0.9	g cm^{-3}

Supplementary Table 3. Compilation of the fraction of Fe_R-OC in TOC (fFe_R-OC) data in different marine environments. The data are presented as means ± standard deviation for each study area.[a]

Marine environments	Study area	Average fFe_R-OC ± SD (%)	Number of data points	Reference
Delta/Estuary	Changjiang Estuary	11.3±3.6	5	Zhao et al., 2018[6]
	East China Sea mobile-muds zone	6.1±2.1	26	Zhao et al., 2018[6]
	Yellow River Estuary	5.7±2.2	9	Sun et al., 2020[7]
	Bohai Sea	11.5±8.3	20	Wang et al., 2019[8]
	Quebec beach subterranean estuary	19.6±20.4	10	Sirois et al., 2018[9]
	Wax Lake Delta	15.1±8.7	37	Shields et al., 2016[10]
	Washington Coast	24.4±8.4	8	Lalonde et al., 2012[11]
	St-Lawrence Estuary	23.1±2.4	3	Lalonde et al., 2012[11]
	St-Lawrence Gulf	23.0±6.0	2	Lalonde et al., 2012[11]
	Mackenzie River delta	7.6	1	Lalonde et al., 2012[11]
Continental shelf	East China Sea	13.2±8.8	12	Ma et al., 2018[12]
	South Yellow Sea	8.8±7.7	10	Ma et al., 2018[12]
	East China Sea offshore regions	9.4±5.1	7	Zhao et al., 2018[6]
	Eurasian Arctic Shelf	11.0±5.5	31	Salvado et al., 2015[13]
	South Yellow Sea	13.0±7.4	27	Tao et al., 2017[14]
	South Yellow Sea	8.7±4.7	10	Sun et al., 2020[7]
	Barents Sea	19.4±6.7	130	Faust et al., 2020, 2021[15, 16]
Continental slope	Madeira turbidite	29.8	1	Lalonde et al., 2012[11]
	Mexican Margin	16.2±7.1	9	Lalonde et al., 2012[11]
	South China Sea[b]	13.3±3.2	57	This study
Deep sea	Southern Ocean	29.0	1	Lalonde et al., 2012[11]
	Station M	14.3±4.1	2	Lalonde et al., 2012[11]
	Equatorial Pacific 0°N	34.8	1	Lalonde et al., 2012[11]
	Equatorial Pacific 9°N	12.2	1	Lalonde et al., 2012[11]
	Okinawa Trough	8.5±3.4	8	Sun et al., 2020[7]

Marine environments	Study area	Average fFe_R-OC ± SD (%)	Number of data points	Reference
Anoxic/sulfidic regions	Black Sea	15.9±12.8	2	Lalonde et al., 2012[11]
	Indian Margin	26.6	1	Lalonde et al., 2012[11]
	Saanich inlet	28.1	1	Lalonde et al., 2012[11]
	Arabian Sea	22.8±5.7	2	Lalonde et al., 2012[11]
	Mexican margin	21.2±2.4	3	Lalonde et al., 2012[11]
Wetland	Min River low salinity wetland	17.9±0.4	12	Bai et al., 2021[17]
	Min River mid salinity wetland	26.7±5.9	12	Bai et al., 2021[17]
	Min River high salinity wetland	28.8±2.2	12	Bai et al., 2021[17]
Mangrove	Philippines Bogtong	14±4	6	Dicen et al., 2018[18]
	Philippines Calauit	11±4	6	Dicen et al., 2018[18]
	Philippines Kodia	10±2	6	Dicen et al., 2018[18]
	Philippines Masinloc	25±9	6	Dicen et al., 2018[18]
	Philippines Oboob	12±2	4	Dicen et al., 2018[18]
	Philippines Subic	15±9	6	Dicen et al., 2018[18]
Tephra	Bering Sea	49.1±27.7	37	Longman et al., 2021[19]
	Northeast Atlantic	36.8±15.9	35	Longman et al., 2024[20]

[a] The most up-to date published dataset compiled by Longman et al., 2022 was used[21], with following exceptions: Ghaisas et al., 2021 was not included for different Fe_R-OC extraction method[22]; Tao et al. 2017 and Longman et al., 2024, which were not included in Longman et al., 2022, were included here[14, 20].

[b] Data derived from SMTZ sediments in QDN-14B in this study are excluded from the calculations, as they are affected by especially strong early diagenesis processes.

Supplementary Table 4 Means of averaged fFe_R-OC of each study area belonging to different marine environments. Means not sharing common letter in the column are significantly different at $P < 0.05$ based on a two-sided Tukey Honest Significant Difference (HSD) test.

Marine environments	Means of averaged fFe_R-OC of each study area (SD)	Number of study cases
Delta/estuary	14.7 (7.3) [a]	10
Continental shelf	11.9 (3.8) [a]	7
Continental slope	19.8 (8.8) [a]	3
Deep sea	19.8 (11.5) [a]	5
Anoxic/sulfidic regions	22.9 (4.8) [a]	5
Wetland	24.5 (5.78) [ab]	3
Mangrove	14.5 (5.5) [a]	6
Tephra	43.0 (8.7) [b]	2

Supplementary Table 5. Global reservoir of Fe_R-OC (Pg C) in Quaternary sediments. The Fe_R-OC reservoir was calculated by multiplying the TOC storage (Pg C) in these three domains by the corresponding average fFe_R-OC in surface sediments.

	Shelf (water depth < 200 m)	Margin (200 m < water depth <3500 m)	Abyss (water depth >3500 m)	Total
TOC storage[a]	2040	43000	100500	28,690±12,165
fFe_R-OC (%)	13.6±6.1	19.8±8.8	19.8±11.5	
Fe_R-OC reservoir	277±124	8,514±3,784	19,899±11,558	

[a]Data from LaRowe et al., 2020[23], where global datasets, including bathymetry, sedimentation rates, TOC content at the sediment-water interface and TOC reactivity were used to model the distribution of OC in Quaternary marine sediments.

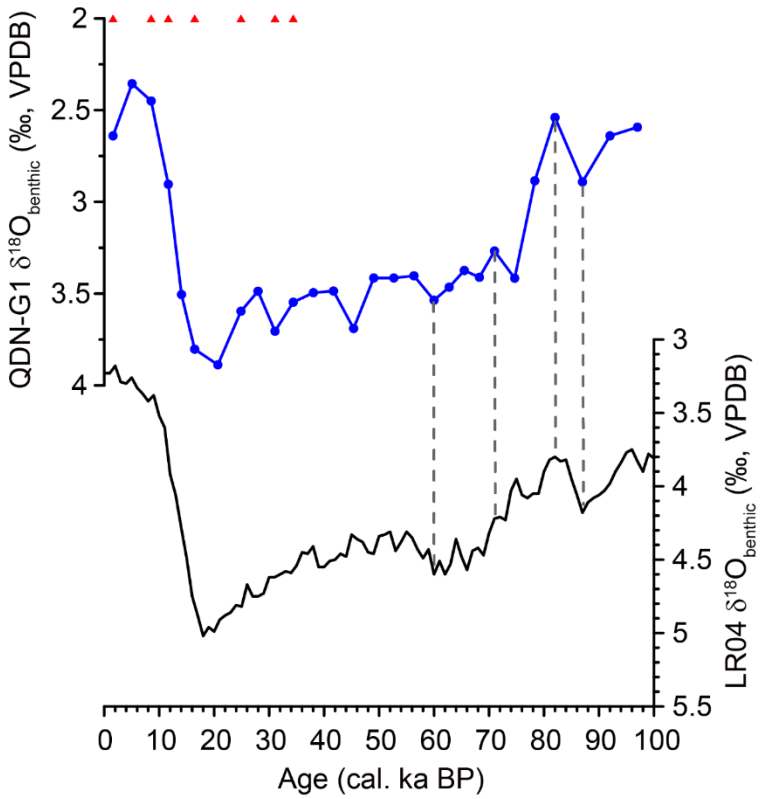

Supplementary Fig. 1. Age model of core QDN-G1. The age model of the upper 4.0 m (0-34.4 ka) was based on 7 accelerator mass spectrometry ^{14}C ages of planktonic foraminifera (*G. ruber*) (red triangles). The age model of the lower 6.8 m (34.4-97.0 ka) was established by aligning the $\delta^{18}O$ record of benthic foraminifera (*C.wuellerstorfi*) (blue line) to the global benthic $\delta^{18}O$ stack LR04[24] (black line). The tie points used for the alignment are indicated by dashed grey lines. See Methods for detailed information. Source data are provided as a Source Data file.

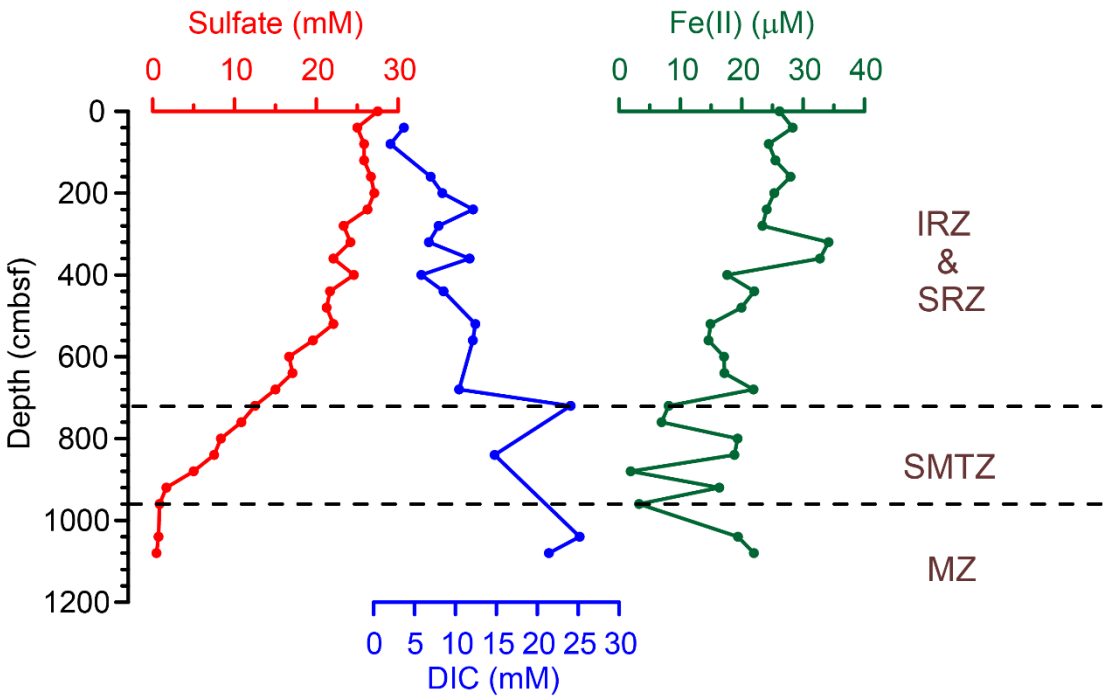

Supplementary Fig. 2. Porewater geochemistry in core QDN-G1. Sulfate, dissolved inorganic carbon (DIC) and Fe(II) concentrations are presented to estimate the location of geochemical horizons, i.e., iron reduction zone (IRZ), sulfate reduction zone (SRZ), sulfate-methane transition zone (SMTZ), and methanogenic zone (MZ). The low concentrations of Fe(II) are consistent with precipitation of Fe(II) with sulfide produced during sulfate reduction, indicating overlapped IRZ and SRZ. Given the data available, the potential upper boundary of SMTZ was determined by abrupt increased DIC at 720 cmbsf. The lower boundary of SMTZ was determined by the depletion of sulfate at 960 cmbsf. Source data are provided as a Source Data file.

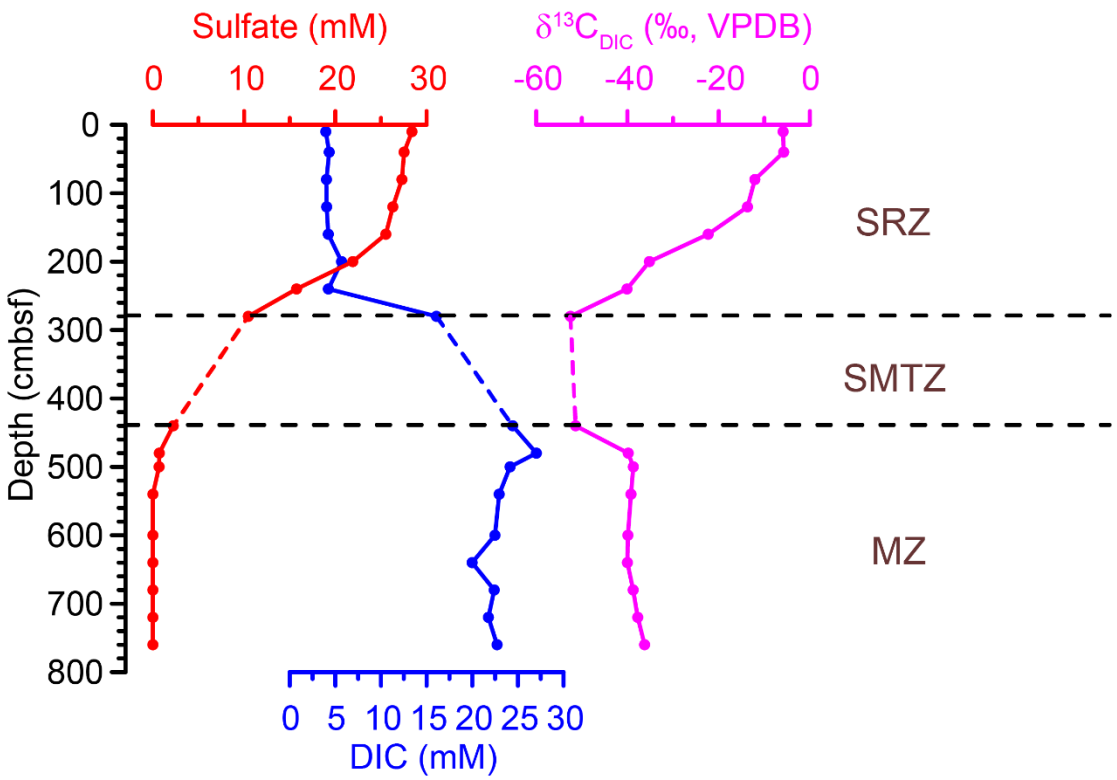

Supplementary Fig. 3. Porewater geochemistry in core QDN-14B. Sulfate concentration, DIC concentration, and DIC carbon isotope ratio ($\delta^{13}C_{DIC}$) are presented to estimate the location of geochemical horizons, i.e., sulfate reduction zone (SRZ), sulfate-methane transition zone (SMTZ), and methanogenic zone (MZ). The estimated upper boundary of SMTZ was determined by increasing DIC concentration and depleted $\delta^{13}C_{DIC}$ at 280 cmbsf. The lower boundary of SMTZ was determined by the depletion of sulfate and low $\delta^{13}C_{DIC}$ at 440 cmbsf. All the data have been published in Niu et al., 2017[25] and Hu et al. (2019)[26]. The data between 300 and 400 cmbsf were suspected to be influenced by seawater during core recovery, and are therefore not presented[25]. Source data are provided as a Source Data file.

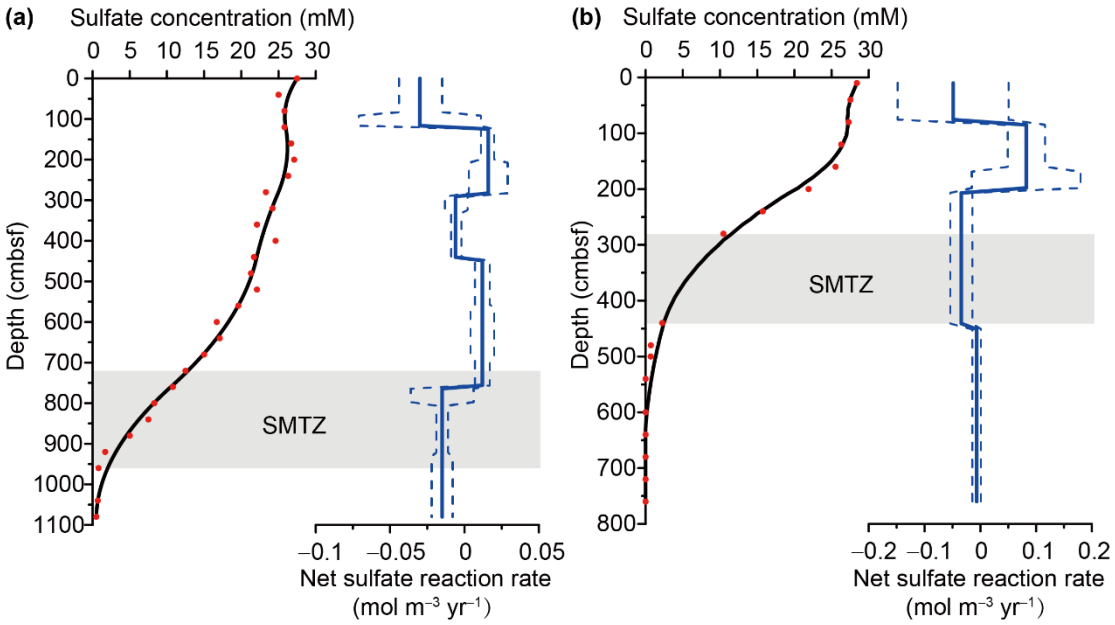

Supplementary Fig. 4. Geochemical modelling of net sulfate reaction rate in cores QDN-G1 (a) and QDN-14B (b). Measured sulfate concentrations are shown in red dots and fitted sulfate concentrations are shown in black lines. A 5-point Gaussian filter was applied to the concentration with the weighting on the 5 points of: [0.06, 0.24, 0.4, 0.24, 0.06][5]. Negative values in modelled net sulfate reduction rates (solid blue line) indicate net consumption, and positive values indicate net production. The 1 σ uncertainty envelope is shown in dashed blue line. Source data are provided as a Source Data file.

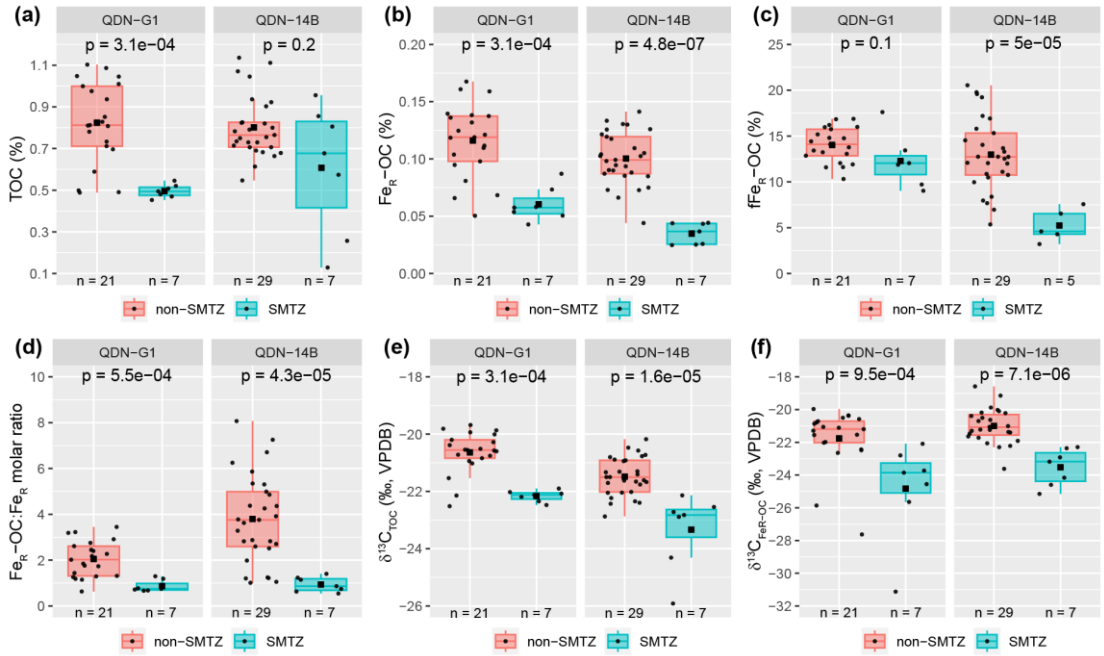

Supplementary Fig. 5 Comparisons of the total organic carbon (TOC) and reactive iron-bound organic carbon (Fe_R-OC) records between non-SMTZ and SMTZ sediments in two cores, including TOC content (a), Fe_R-OC content (b), fraction of Fe_R-OC in TOC (fFe_R-OC) (c), Fe_R-OC to Fe_R molar ratio (d), carbon isotope ratio of TOC (e), and carbon isotope ratio of Fe_R-OC (f). fFe_R-OC data at 410 and 420 cmbsf in QDN-14B are biased by extremely low TOC and are not included for analysis. Significant levels in two-sided Wilcoxon rank sum test are shown. Box plots indicate mean (solid square), median (middle line), 25th, 75th percentile (box) and 1.5 times interquartile range (whiskers) with data points (solid dots) overlapped on top. Source data are provided as a Source Data file.

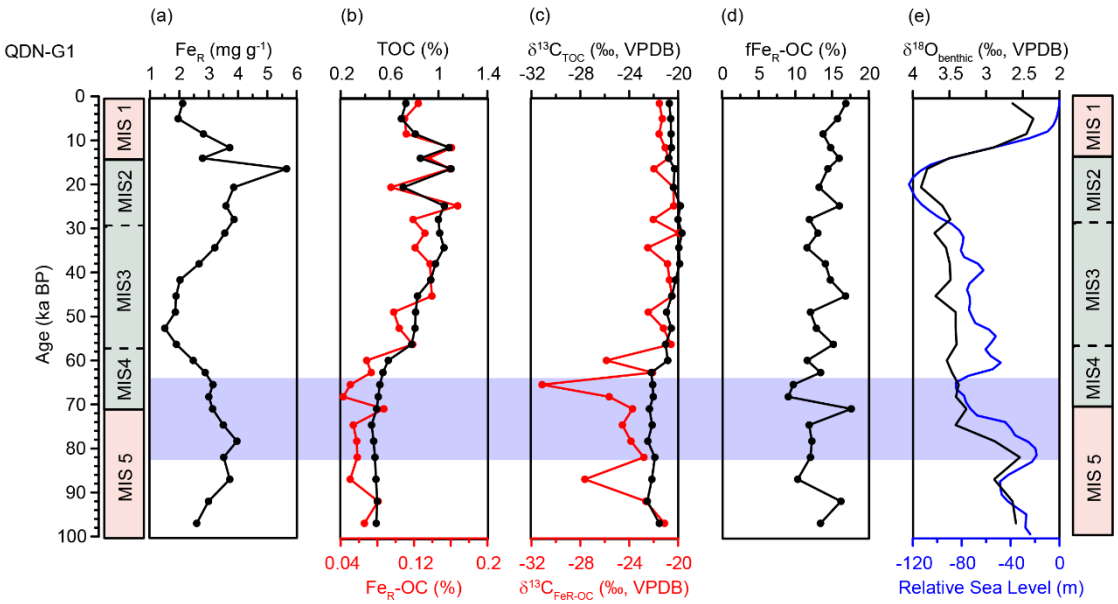

Supplementary Fig. 6. Content and carbon isotope ratios of TOC and Fe$_R$-OC in core QDN-G1 over glacial-interglacial cycles. The pink and green bars indicate interglacial periods and the last glacial period, respectively. (a) Content of Fe$_R$. (b) Content of TOC (black line) and Fe$_R$-OC (red line). Separate x-axes are used for TOC and Fe$_R$-OC, labelled in the same color as the data profile. (c) Carbon isotope ratios of TOC (black line) and Fe$_R$-OC (red line). Separate x-axes are used for TOC and Fe$_R$-OC, labelled in the same color as the data profile. (d) The fraction of Fe$_R$-OC in TOC (fFe$_R$-OC). (e) $\delta^{18}O$ record of benthic foraminifera (black line) and global relative sea level record from Waelbroeck et al, 2002[27] (blue line). Separate x-axes are used for $\delta^{18}O$ record of benthic foraminifera and relative sea level record, labelled in the same color as the data profile. The location of the SMTZ is highlighted in purple. Source data are provided as a Source Data file.

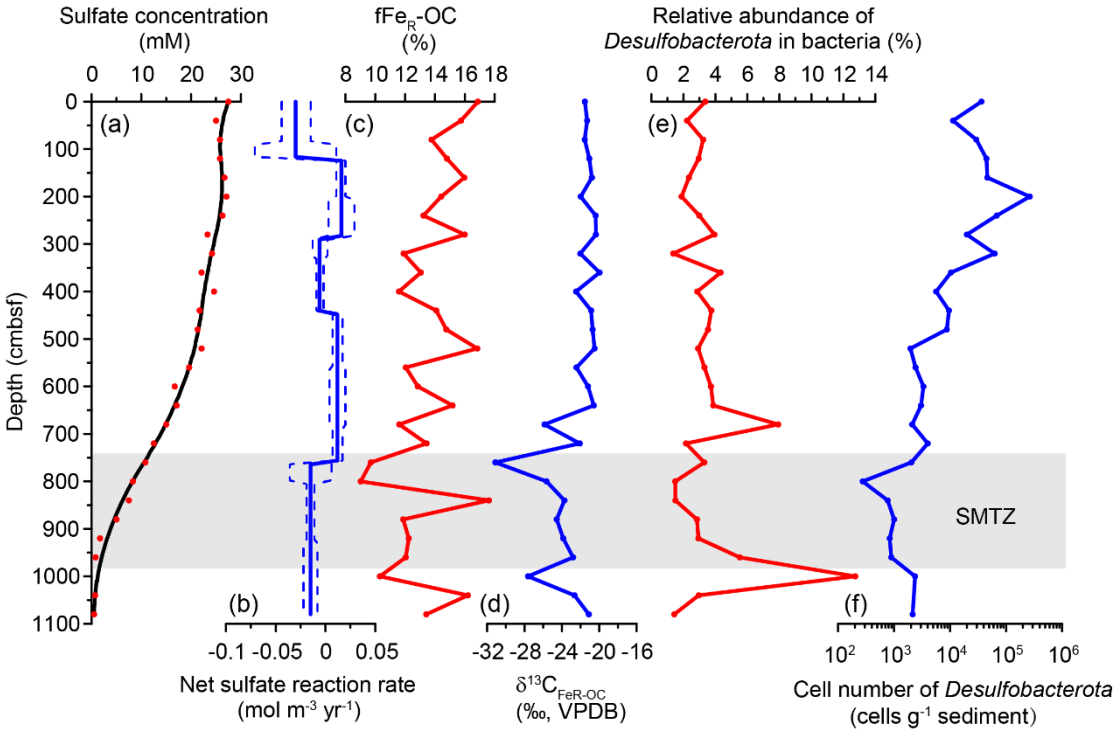

Supplementary Fig. 7. Geochemical modelling and microbial evidence show that low sulfate reduction rate results in moderate decrease in fFe_R-OC in the SMTZ of core QDN-G1. (a) Measured (red dots) and fitted (black line) sulfate concentrations. A 5-point Gaussian filter was applied to the concentration with the weighting on the 5 points of: [0.06, 0.24, 0.4, 0.24, 0.06][5]. (b) Modelled net reaction rate profile of sulfate. Negative values indicate net consumption, and positive values indicate net production. The 1 σ uncertainty envelope is shown in dashed line. (c) Down-core record of fFe_R-OC. (d) Downcore record of $\delta^{13}C_{FeR\text{-}OC}$. (e) Relative abundance of *Desulfobacterota* in bacteria, to which the most of the sulfate-reducing bacteria belong[28]. (f) The cell number of *Desulfobacterota*, translated from the cell number of bacteria by multiplying the relative abundance of *Desulfobacterota* in bacteria. The gray bar shows the position of SMTZ. Source data are provided as a Source Data file.

Supplementary references

1. Cartapanis, O., Bianchi, D., Jaccard, S. L. & Galbraith, E. D. Global pulses of organic carbon burial in deep-sea sediments during glacial maxima. *Nat. Commun.* **7**, 10796 (2016).
2. Fontugne, M. R. & Calvert, S. E. Late Pleistocene variability of the carbon isotopic composition of organic matter in the Eastern Mediterranean: Monitor of changes in carbon sources and atmospheric CO_2 concentrations. *Paleoceanography* **7**, 1-20 (1992).
3. He, J., Zhao, M., Li, L., Wang, P. & Ge, H. Sea surface temperature and terrestrial biomarker records of the last 260 ka of core MD05-2904 from the northern South China Sea. *Chin. Sci. Bull.* **53**, 2376-2384 (2008).
4. Kienast, M., Calvert, S. E., Pelejero, C. & Grimalt, J. O. A critical review of marine sedimentary $\delta^{13}C_{org}$-pCO_2 estimates: New palaeorecords from the South China Sea and a revisit of other low-latitude $\delta^{13}C_{org}$-pCO_2 records. *Global Biogeochemical Cycles* **15**, 113-127 (2001).
5. Wang, G., Spivack, A. J., Rutherford, S., Manor, U. & D'Hondt, S. Quantification of co-occurring reaction rates in deep subseafloor sediments. *Geochim. Cosmochim. Acta* **72**, 3479-3488 (2008).
6. Zhao, B. et al. The Role of Reactive iron in the preservation of terrestrial organic carbon in estuarine sediments. *J. Geophys. Res. Biogeosci.* **123**, https://doi.org/10.1029/2018JG004649 (2018).
7. Sun, C.-H. et al. Examining bulk and iron-associated organic carbon through depth in margin sea sediments (China) under contrasting depositional settings: Chemical and NEXAFS spectral characterization. *J. Mar. Syst.* **207**, 103344 (2020).
8. Wang, D., Zhu, M. X., Yang, G. P. & Ma, W. W. Reactive iron and iron‐bound organic carbon in surface sediments of the river‐dominated Bohai Sea (China) versus the Southern Yellow Sea. *J. Geophys. Res. Biogeosci.* **124**, 79-98 (2019).
9. Sirois, M., Couturier, M., Barber, A., Gelinas, Y. & Chaillou, G. Interactions between iron and organic carbon in a sandy beach subterranean estuary. *Mar. Chem.* **202**, 86-96 (2018).
10. Shields, M. R., Bianchi, T. S., Gélinas, Y., Allison, M. A. & Twilley, R. R. Enhanced terrestrial carbon preservation promoted by reactive iron in deltaic sediments. *Geophys. Res. Lett.* **43**, 1149-1157 (2016).
11. Lalonde, K., Mucci, A., Ouellet, A. & Gélinas, Y. Preservation of organic matter in sediments promoted by iron. *Nature* **483**, 198-200 (2012).
12. Ma, W.-W., Zhu, M.-X., Yang, G.-P. & Li, T. Iron geochemistry and organic carbon preservation by iron (oxyhydr)oxides in surface sediments of the East China Sea and the south Yellow Sea. *J. Mar. Syst.* **178**, 62-74 (2018).
13. Salvadó, J. A. et al. Organic carbon remobilized from thawing permafrost is resequestered by reactive iron on the Eurasian Arctic Shelf. *Geophys. Res. Lett.* **42**, 8122-8130 (2015).
14. Tao, J., Ma, W., Li, W., Li, T. & Zhu, M. Organic carbon preservation by reactive iron oxides in South Yellow Sea sediments. *Haiyang Xuebao* **39**, 16-24 (2017).
15. Faust, J. C. et al. Millennial scale persistence of organic carbon bound to iron in Arctic marine sediments. *Nat. Commun.* **12**, 275 (2021).
16. Faust, J. C. et al. Does Arctic warming reduce preservation of organic matter in Barents Sea sediments? *Philosophical Transactions of the Royal Society A: Mathematical, Physical and Engineering Sciences* **378**, 20190364 (2020).

17. Bai, J. et al. Iron-bound carbon increases along a freshwater−oligohaline gradient in a subtropical tidal wetland. *Soil Biol. Biochem.* **154**, 108128 (2021).
18. Dicen, G. P., Navarrete, I. A., Rallos, R. V., Salmo, S. G. & Garcia, M. C. A. The role of reactive iron in long-term carbon sequestration in mangrove sediments. *J. Soils Sed.*, 1-10 (2018).
19. Longman, J., Gernon, T. M., Palmer, M. R. & Manners, H. R. Tephra deposition and bonding with reactive oxides enhances burial of organic carbon in the Bering Sea. *Global Biogeochemical Cycles* **35**, e2021GB007140 (2021).
20. Longman, J. et al. Production and preservation of organic carbon in sub-seafloor tephra layers. *Mar. Chem.* **258**, 104334 (2024).
21. Longman, J., Faust, J. C., Bryce, C., Homoky, W. B. & März, C. Organic carbon burial with reactive iron across global environments. *Global Biogeochemical Cycles* **36**, e2022GB007447 (2022).
22. Ghaisas, N. A., Maiti, K. & Roy, A. Iron-mediated organic matter preservation in the Mississippi River-influenced shelf sediments. *J. Geophys. Res. Biogeosci.* **126**, e2020JG006089 (2021).
23. LaRowe, D. E. et al. Organic carbon and microbial activity in marine sediments on a global scale throughout the Quaternary. *Geochim. Cosmochim. Acta* **286**, 227-247 (2020).
24. Lisiecki, L. E. & Raymo, M. E. A Pliocene‐Pleistocene stack of 57 globally distributed benthic $\delta^{18}O$ records. *Paleoceanography* **20**, PA1003 (2005).
25. Niu, M., Fan, X., Zhuang, G., Liang, Q. & Wang, F. Methane-metabolizing microbial communities in sediments of the Haima cold seep area, northwest slope of the South China Sea. *FEMS Microbiol. Ecol.* **93**, fix101 (2017).
26. Hu, Y. et al. Pore fluid compositions and inferred fluid flow patterns at the Haima cold seeps of the South China Sea. *Mar. Pet. Geol.* **103**, 29-40 (2019).
27. Waelbroeck, C. et al. Sea-level and deep water temperature changes derived from benthic foraminifera isotopic records. *Quaternary Science Reviews* **21**, 295-305 (2002).
28. Müller, A. L., Kjeldsen, K. U., Rattei, T., Pester, M. & Loy, A. Phylogenetic and environmental diversity of DsrAB-type dissimilatory (bi)sulfite reductases. *ISME J.* **9**, 1152-1165 (2015).